Available online at www.sciencedirect.com
ScienceDirect
Surface Science 601 (2007) 1246–1254
SURFACE SCIENCE
www.elsevier.com/locate/susc

Coverage dependence of finite temperature quantum distribution of hydrogen on nickel(0 0 1) surface

Markku Leino *, Ilkka Kylänpää, Tapio T. Rantala

Institute of Physics, Tampere University of Technology, P.O. Box 692, FI-33101 Tampere, Finland

Received 25 September 2006; accepted for publication 12 December 2006
Available online 30 December 2006

Abstract

Finite temperature quantum behavior of hydrogen adsorbates on Ni(0 0 1) surface is simulated using path-integral Monte Carlo technique. The adsorbate–surface and adsorbate–adsorbate interactions are described by the many-body alloy potential form, fitted to the adsorption parameters from DFT calculations. Temperatures 100 K and 300 K and coverages from 1/8 to 7/8 are considered. Also quantum and classical adsorbate behavior is compared.

At low temperatures, the quantum delocalization of the adsorbates is considerable with all studied coverages, and therefore, temperature dependence of distributions is weak. At $T = 300$ K, however, the H–H interaction energy has a considerable effect on distributions and energetics. By using a semi-classical description of the hydrogen adsorbates both temperature and coverage dependencies become strong at both temperatures.
© 2006 Elsevier B.V. All rights reserved.

Keywords: Monte Carlo simulations; Nickel; Construction and use of effective interatomic interactions; Equilibrium thermodynamics and statistical mechanics; Quantum effects; Hydrogen molecule

1. Introduction

Hydrogen motion and interactions on metal surfaces are of interest both technologically and fundamentally. Hydrogen interactions are considered to be simple and therefore well suited for fundamental research [1]. In particular, the light mass of hydrogen emphasizes quantum effects [2–5], which are used to explain peculiar adsorbate diffusion [6–12], vibrational observations [6], electron-energy loss spectra [13,14], low-energy electron diffraction [13,14], photoemission [14], helium scattering [15], thermal desorption [7], linear optical diffraction [16] and field emission [16,17]. Furthermore, it has been shown that quantum effects are essential in understanding the phenomena of H interactions on Ni surface [11,13,18], and, H on metal surfaces provides a unique opportunity to observe the crossover from quantum to classical dynamics at elevated temperatures [5]. Finally, combination of the many-body aspect of the interactions and the quantum nature of hydrogen dynamics at low temperatures [2] makes this system even more interesting.

Many of the interesting quantum states relate to Ni(0 0 1) surface, where H adsorbate is known to delocalize and develop a two-dimensional band structure. Thus, the protonic band structure may be important [4,19] in order to understand hydrogen reactions on metal surfaces. Many questions are still open, e.g., to what extent the electronic structure of the surface influences the reaction of atomic H (D) with adsorbed H or D [20]. Also, it is known, that presence of an adsorbate on a surface can profoundly change the surface reactivity [21]. The dissociative adsorption of molecules on surfaces of solids is of central importance in surface catalysis and has been extensively studied both experimentally and theoretically [22].

At low temperatures, the quantum delocalization of the hydrogen adsorbate on a Ni(1 0 0) surface is considerable,

* Corresponding author. Tel.: +358 50 363 8659; fax: +358 3 3115 2600.
E-mail addresses: Markku.Leino@tut.fi (M. Leino), Tapio.Rantala@tut.fi (T.T. Rantala).

0039-6028/$ - see front matter © 2006 Elsevier B.V. All rights reserved.
doi:10.1016/j.susc.2006.12.068

as we have shown earlier, see Ref. [18], and therefore, temperature dependence of distributions is weak. By using a classical description of the hydrogen adsorbate temperature dependence of the distributions and energetics becomes strong at all temperatures, proving that quantum description is necessary for the correct picture of H/Ni(0 0 1) system. At room temperature, $T = 300$ K, the extensive classical distribution is quite similar to that of quantum case and the classical thermal spreading conceals the quantum delocalization. It was found that the classical distributions are more bridge-direction oriented compared with the quantum case, where tunneling allows more circular shape.

Mutual interaction between adsorbed hydrogen atoms may significantly alter the apparent temperature dependence of the diffusion [23], and thus, other properties of the system. Two of the interaction mechanisms are direct, through space, and two are indirect, through substrate [24]: dipole–dipole interaction, direct overlap between adsorbate electronic levels, indirect interaction mediated by the non-rigid substrate ion cores and indirect interaction mediated by the metal electrons. The electrostatic interaction is assumed to be repulsive between hydrogen adatoms at Ni surface [25].

Some Ni surfaces exhibit ordered superstructures for H_n [26], but none is found for (1 0 0) surface [1,25]. On some surfaces, a molecular adsorbate is observed, e.g., Ni(5 1 0) surface covered with a dense atomic-hydrogen layer [27], but as Mårtensson et al. [27] pointed out, EELS studies of hydrogen adsorption on the flat Ni(1 0 0) surface shows that there is no molecular adsorption state populated at 80 K substrate temperature.

We report here fully quantum mechanical and thermally averaged constant temperature path-integral Monte Carlo simulation (PIMC) of hydrogen atoms on a rigid Ni(1 0 0) surface. The method is described in detail in Ref. [18] for the case of single H atom. Here we consider the coverages from 1/8 to 7/8. By employing PIMC method, we evaluate the finite temperature many-body density distributions and related energetics for quantum mechanical and classical cases. We compare the results to the semi-classical "atoms at the adsorption sites" picture. We assess the quantum nature and temperature dependencies of the hydrogen distribution and differences with the semi-classical picture. In particular, hydrogen–hydrogen interactions are considered in terms of pair correlation functions and energetics.

In the next chapter, the many-body alloy potential and PIMC are briefly described, chapter 3 gathers the results together and, finally, the last chapter presents the conclusions.

2. Computational methods

For the simulation, we need the full many-dimensional potential-energy hypersurface for several interacting H atoms at the surface. Therefore, we have chosen MBA potential, reviewed in Subsection 2.1, to describe Ni–Ni, Ni–H and H–H interactions. In Subsection 2.2 the path-integral method is described.

2.1. Many-body alloy potential

MBA has been succesfully used for H/Pd systems and for studies of the electronic and structural properties of small clusters [28,29], surfaces of metals, dilute metal alloys, see Ref. [30] and references therein, and the finite temperature quantum distribution of H adsorbate on Ni(0 0 1) surface [18].

The total (cohesive) energy of a crystal or a cluster in MBA description is decomposed [30,31] into individual atomic contributions E_i as

$$E_{\mathrm{T}} = \sum_i E_i, \tag{1}$$

where i runs over all atoms in the system and

$$E_i = -\sqrt{\sum_{j\neq i} \xi_{\alpha\beta}^2 \exp\left[-2q_{\alpha\beta}\left(\frac{r_{ij}}{r_{0,\alpha\beta}} - 1\right)\right]} + \sum_{j\neq i} \epsilon_{\alpha\beta} \exp\left[-p_{\alpha\beta}\left(\frac{r_{ij}}{r_{0,\alpha\beta}} - 1\right)\right]. \tag{2}$$

The attractive part (first term) is due to the hybridization of orbitals. It is based on a parametrized tight-binding Hamiltonian and the second-moment approximation. The repulsive part (second term) is parametrized as a pair-wise Born–Mayer potential with an exponential distance dependence [31].

We have fitted MBA potential to describe interactions between H adsorbate and Ni atoms [18]. The bulk Ni–Ni parameters were fitted to the lattice constant $a = 3.52$ Å, the nearest neighbour distance $r_0 = 2.49$ Å, cohesive energy $E_{\mathrm{coh}} = -4.44$ eV and bulk modulus $B = 1.17$ eV/Å^3. The H–Ni parameters of MBA potential were fitted to the DFT data given by Mattsson et al. [12]. The fitted quantities are the adsorption energy of the hollow site, $E_{\mathrm{ads}} = 2.8$ eV, the equilibrium distance from the surface at hollow site $r_a = 0.5$ Å and the energy barrier between the hollow sites through the bridge site, $E_{\mathrm{barr}} = 0.14$ eV. For DFT details, see Ref. [12].

For the H_2 dimer in MBA scheme we adopt the parameters from Ref. [31], giving the binding energy as -4.95 eV at bond length 0.9 Å. We note that the parameters are not fitted to describe the free H_2 molecule but the one adsorbing onto on a transition metal surface.

All of the MBA parameters that are used in simulations of this paper are given in Table 1.

Table 1
Many-body alloy (MBA) potential parameters for all atom pairs in Eq. (2)

X_α–X_β	$q_{\alpha\beta}$	$p_{\alpha\beta}$	$r_{0,\alpha\beta}$ [Å]	$\epsilon_{\alpha\beta}$ [eV]	$\xi_{\alpha\beta}$ [eV]
H–H	3.22	5.28	2.30	0.16	0.91
H–Ni	2.87	5.87	1.44	2.70	5.52
Ni–Ni	3.00	8.62	2.49	0.20	1.97

2.2. Path-integral Monte Carlo method

Quantum treatment at the finite temperature is included by using path-integral formalism for hydrogen atoms with Monte Carlo scheme, and by calculating the trace of finite temperature quantum density matrix

$$Z = \left(\frac{mM}{2\pi\hbar^2\beta}\right)^{d/2} \int \exp\left[-\beta \sum_{n=1}^{M} (K(r_{n-1}, r_n) + U(r_{n-1}, r_n))\right] \mathrm{d}r_0 \ldots \mathrm{d}r_{M-1}, \tag{3}$$

where functions K and U define internal and external energies of the system. In the primitive approximation [32,33] they are written as

$$K(r_{n-1}, r_n) = \frac{mM}{2\hbar^2\beta^2}(r_{n-1} - r_n)^2 \tag{4a}$$

and

$$U(r_{n-1}, r_n) = \frac{1}{2M}(V(r_{n-1}) + V(r_n)), \tag{4b}$$

where m is the mass of the particle and M, large enough integer, is called the Trotter number. The periodic boundary conditions in imaginary time are taken into use, i.e., $r_0 = r_M$ [18].

Quantum description is complete at the limit, where the Trotter number $M \to \infty$. However, the distributions and expectation values converge at some finite Trotter number, which depends on the temperature and external potential. This is clearly seen from the quantum distributions at different Trotter numbers, and by testing the procedure for analytically solvable systems. We found sufficient convergence in our case with Trotter number $M = 64$. At 100 K, this can be considered as a compromise with computational labour, but shows good convergence at 300 K. The typical number of sufficient Monte Carlo steps is about 10^8 for classical simulations and 2×10^9 for $T = 100$ and 4×10^8 for $T = 300$ K quantum simulations. Also, a similar sampling is needed in quantum cases to reach the equilibrium states. For higher H coverages, we are not able to use high enough Trotter numbers. Therefore, we choose $M = 1$ that returns the PIMC to classical Metropolis Monte Carlo approach. On the other hand, this allows us to compare classical and quantum hydrogen adsorbates.

Our surface model is a periodic slab of six layers of Ni atoms, eight atoms in each layer, including total of 48 atoms. The lateral periodicity is two lattice constants, $2a$. See Fig. 1. Some structure related data of the model is collected into Table 2.

3. Results

First, we test the performance of MBA potential in the present case, which now involves H–H interaction at the surface, in addition to previously reported H–Ni and Ni–Ni parametrizations [18]. This is done by considering the s.c. H_2 molecule dissociation elbow plots. Also, surface relaxation is considered, though computing capacity does not allow us to include Ni atom dynamics here, as was done in our previous study with the single hydrogen atom [18]. Then, we consider the equilibrium distributions and pair correlation functions of hydrogen atoms as a function of coverage. For lower coverages, we are able to consider both quantum and classical hydrogen and compare these, whereas, for higher coverages, we simulate the classical hydrogen only. Finally, we discuss the energetics in the above cases.

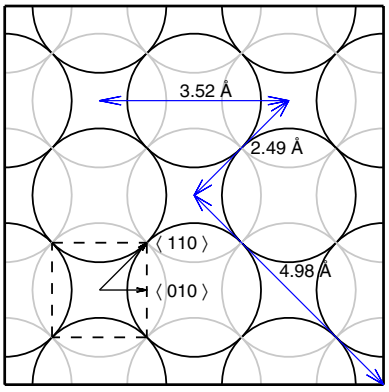

Fig. 1. Simulation supercell of Ni(001) surface (of FCC lattice, $a = 3.52$ Å) schematically, surface and subsurface layer atoms indicated by black and grey circles, respectively. One of the four-fold hollow sites is designated by the dashed square and the high symmetry directions along the surface are shown. The three possible hollow site distances (within the "periodical" simulation cell) are depicted.

Table 2
Comparison of hollow site pairs defined in Fig. 1

		R [a]	R [Å]	N_{fcc}	N_{sim}	ΔE [meV]
HBH	⟨110⟩	$\sqrt{1/2}$	2.49	4	4	199
HTH	⟨100⟩	1	3.52	4	2	99
	⟨110⟩	$\sqrt{2}$	4.98	4	1	1

N_{sim} and N_{fcc} give the statistical weight of the pairs in case of our periodic model and real (001) surface of FCC lattice, respectively, as seen in the pair correlation function of H atoms in hollow sites. HBH and HTH refer to the related elbow plots in Fig. 2.

3.1. H–H interaction in MBA

The MBA parameters for H–Ni were fitted to the case of single hydrogen atom adsorption in our previous study [18] using the DFT data of Mattson et al. [12], while the H–H parameters are taken directly from Ref. [31]. Thus, the combination should be tested against a good reference before use. For this purpose, we consider the high-symmetry potential-energy hypersurfaces conventionally used to illustrate the dissociation dynamics of H_2 molecule coming down to the perfect and rigid surface. Due to their typical shape, they are called "elbow plots". We choose the DFT calculations of Kresse et al. [25] to compare with.

It should be pointed out that description of such indirect interactions are not straightforward, as H–H interactions may be sensitive to the character of the H-induced surface

electronic structure involving the transition-metal d states [24]. On the other hand, the detailed form of the metal DOS was shown to be not important for a description of adsorbate photoemission [34]. However, different binding energies of H atoms at different sites on the surface due to the H–H interactions [26] put forward a challenge for MBA.

We present a set of MBA elbow plots in Figs. 2–4. These should be compared to those of Kresse et al., and also, to the equipotential contour lines of single hydrogen atom on Ni surface [18]. We see that MBA surprisingly successfully transforms the single atom PES to the various elbow plots as a consequence of H–H interaction.

In our case, the most important regions of the elbow plots to consider are the hollow sites shown in Fig. 2, where hydrogen adsorbates almost exclusively dwell in thermal equilibrium. Fig. 2a shows the PES for H_2 molecule dissociation above the bridge site towards the hollow sites (HBH). A small physisorption energy minimum of 20 meV is found in agreement with DFT data of Kresse [35]. We evaluate for the dissociation barrier a value of 140 meV, as the DFT barrier is 110 meV.

The chemisorption minimum is at 0.5 Å, the same as in the single-adsorbate case. The distance between adsorbed hydrogen atoms at the chemisorption minimum is 2.7 Å, expressing a repulsion between adjacent adsorbates. This repulsion is about 200 meV, see Table 3, and it is not present in DFT results.

The H–H MBA parameters are not intended for description of free H_2 molecule: the dissociation energy is too large

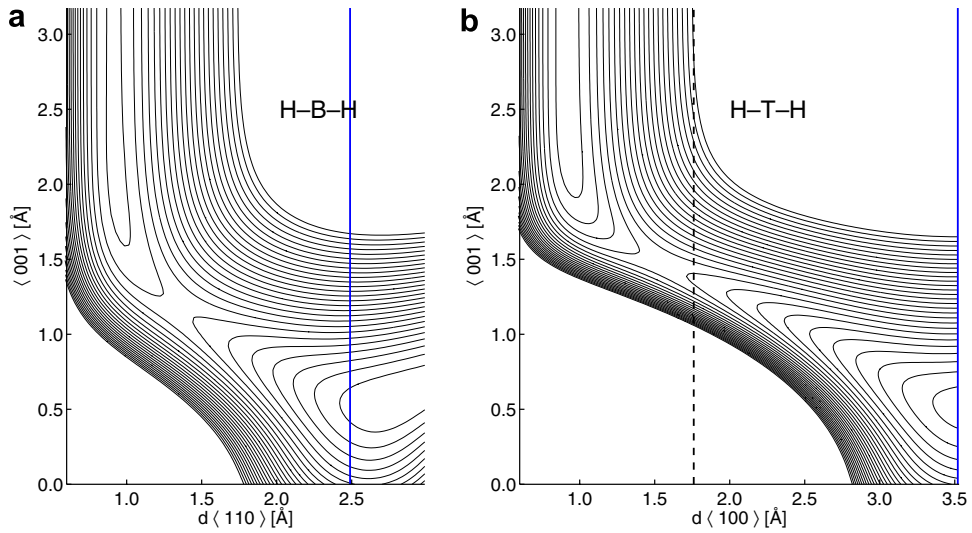

Fig. 2. Elbow plots for H_2 dissociation to hollow sites from MBA potential. High symmetry cases in planes {1 1 0} (on bridge site) and {0 1 0} (on top site) are shown on the left and right, respectively. Line spacing is 100 meV. Note that the minimum is about 100 meV higher in the former case due to the difference in remaining indirect H–H interation; see text.

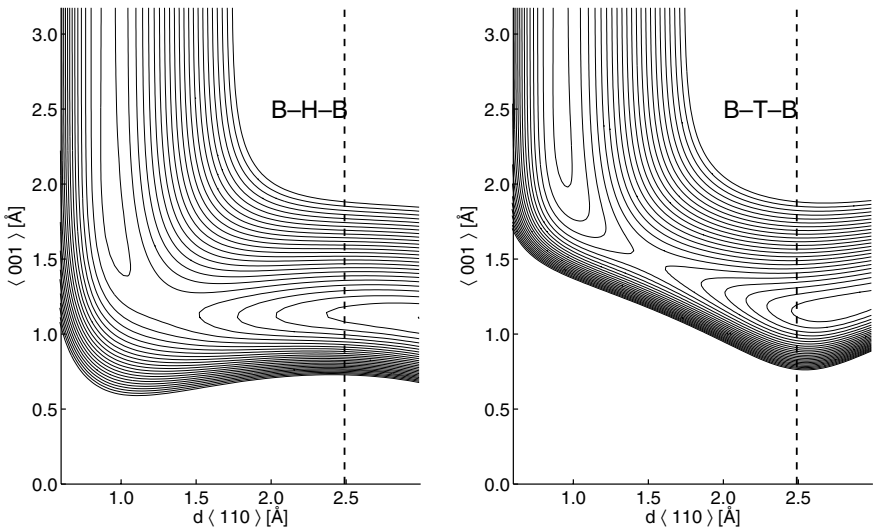

Fig. 3. Elbow plots for H_2 dissociation to bridge sites from MBA potential. High symmetry cases in planes {1 1 0} (on hollow site) and {1 1 0} (on top site) are shown on the left and right, respectively. Line spacing is 100 meV. Again, the minima differ due to the difference in remaining indirect H–H interation.

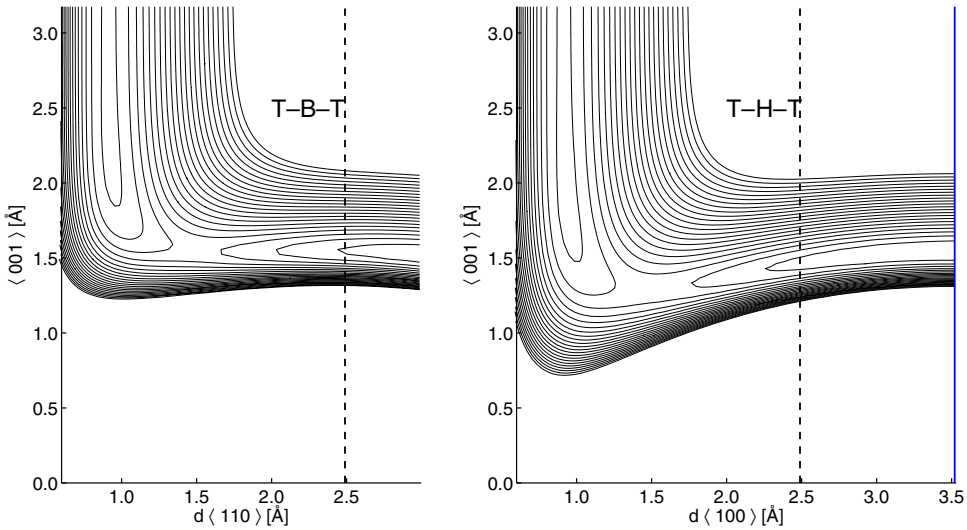

Fig. 4. Elbow plots for H_2 dissociation to top sites from MBA potential. High symmetry cases in planes {1 1 0} (on bridge site) and {1 0 0} (on hollow site) are shown on the left and right, respectively. Line spacing is 100 meV.

Table 3
MBA H_2 molecule physisorption, dissociation barrier and chemisorption energetics for the elbow plots in Fig. 2, compared to the DFT energetics from Ref. [35]

		Physisorption			Chemisorption	
		(d, z) [Å]	E [meV]	E_{dis} [meV]	(d, z) [Å]	E [eV]
MBA	hbh	(0.9,–)	25	140	(2.8,0.5)	0.5
	hth	(0.9,–)	50	350		0.6
DFT	hbh	(0.8,–)	20	110	(2.5,0.5)	1.1
	hth		20	0		

by about 0.5 eV. Therefore, the chemisorption energy becomes too small by about the same amount.

The elbow plot above the top site towards hollow sites (HTH), Fig. 2b, presents the same features as HBH. The only essentially difference in these two cases is the H–H repulsion, see Table 3. H atoms in hollow sites further apart do not essential interact, see ΔE in Table 3. We note that the dissociation barrier is not described correctly, but it is not relevant for the equilibrium distribution of H adsorbates at low coverages.

The four elbow plots in Figs. 3 and 4 are shown to illustrate performance of MBA, though they are not essential in our room temperature equilibrium simulations.

It is interesting to test MBA performance in description of surface relaxation. By allowing two uppermost Ni layers to relax, their separation is changed by $\Delta z_{12} = -0.120$ Å, which is close to the DFT result [25] −0.116 Å. Also, for the second layer separation change we get $\Delta z_{23} = -0.08$ Å, a negative value indicating a smaller layer separation. The corresponding DFT value is $\Delta z_{23} = 0.04$ Å.

As a conclusion, we find MBA with the given parameters capable of describing a single and two interacting H atoms on a Ni surface, and assume its validity for higher coverages too. Furthermore, it seems to describe correctly many other features of the system that are not relevant or needed in the present study.

3.2. Hydrogen adsorbates on nickel surface

First, we describe the adsorbate distributions for hydrogen coverages from 1/8 to 7/8 on Ni(1 0 0) surface. Temperature and quantum effects and also the H–H interactions are considered. The adsorbate energetics are estimated in the next section.

As was pointed out earlier, the simulation cell is of finite size and periodic, with periodicity of $2a$, see Fig. 1. Due to this, in $\langle 1\,0\,0 \rangle$ and $\langle 1\,1\,0 \rangle$ directions there are only two and one hollow site distances, respectively, see Fig. 1. Thus, the finite simulation cell is different from the infinite one, as indicated in Table 2.

The hydrogen quantum distribution in the hollow site at low coverages and low temperatures does not strongly depend on the coverage nor on the actual temperature. It is rather similar to that at zero Kelvin [12–14]. We confirm this fact and illustrate it in Fig. 5 with the distributions from 100 K and 300 K with hydrogen adsorbate coverages varying from 1/8 to 4/8. Indeed, only a slight spreading of the distributions can be observed when increasing the temperature, and thus, the difference between the shown two is almost insignificant.

At $T = 100$ K, the adsorbates are lying in the "circular ground state", exhibiting harmonic confinement. It should be noted that at $T = 100$ K, the distributions of coverages $\theta = 2/8$ and $\theta = 3/8$ are almost identical. Thus, the adsorbate–adsorbate interaction is rather small in both cases, though the pair correlation function differs, see below. At coverage $\theta = 2/8$, the spatial width of distribution is smallest; the hydrogen is most localized.

Only at coverages $\theta \geqslant 4/8$ the lateral distribution of quantum adsorbates is profoundly different from zero-

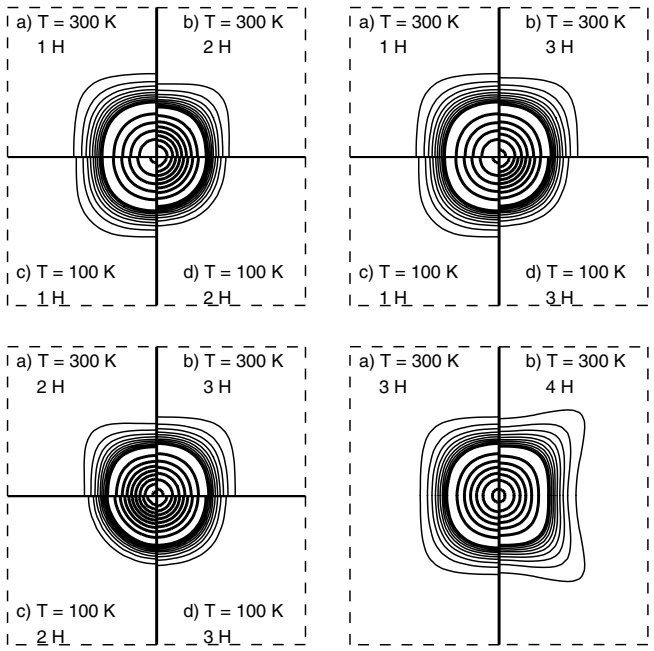

Fig. 5. One-particle quantum distribution in the hollow site, see Fig. 1, in case of adsorbate covarages $\theta = 1/8$, 2/8, 3/8, and 4/8 in the simulation cell and for temperatures 100 K and 300 K. The equidensity contours present the three-dimensional density projected onto the surface plane, i.e., integrated over z-direction. The thin and thick lines show densities 0.5, 1.0, 1.5, ... and 5, 10, 15, ... atoms/(surface) unit cell.

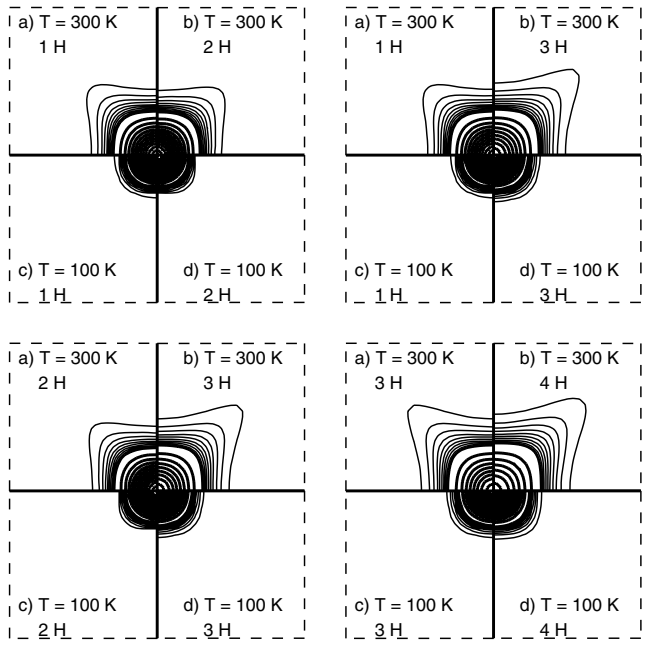

Fig. 6. "Classical hydrogen" distributions corresponding to those of quantum hydrogen in Fig. 5. Notations are the same as in Fig. 5.

Kelvin distributions, see subfigure in low-right corner in Fig. 5, showing more towards bridge-site orientation. This may be a reflection of attractive interaction [23] of H adsorbates at HTH configuration, see Fig. 2b. We have not been conducted the simulations at $T = 100$ K for coverages $\theta > 3/8$ due to the required computer capacity.

The "classical hydrogen adsorbates" show more pronounced temperature effect, see Fig. 6. It is due to the absence of zero-point vibration at $T = 100$ K, the distribution is spherical (harmonic confinement) and at room temperature, it is oriented towards bridge site. At $T = 300$ K, the thermal spreading conceals the classical in all studied coverages. Here too, the coverage $\theta = 2/8$ exhibits minimum in spatial width, following from the repulsive interaction of the H adsorbates. The lateral distributions of quantum and classical adsorbates at room temperature are quite similar, the largest difference being that the classical distributions are more bridge-direction oriented.

The pair correlation functions of the distributions, (see Fig. 7), show that all hydrogen adsorbates tend to reside apart from each other, which, again, is an indication of H–H repulsion. Thus, there is no molecular adsorption state at $T = 300$ K or $T = 100$ K, a result observed for $T = 80$ K by Mårtensson et al. [27]. The maximum values of pair correlation functions are obtained at hollow-site distances, 3.5 Å and 5.0 Å.

At higher coverages, $\theta \geqslant 3/8$, the hydrogen adsorbates are compelled to be closer to others, leading to a large peak at the distance of 3.5 Å. The difference on the quantum pair correlation functions for $\theta = 2/8$ and $\theta = 3/8$ in Fig. 7 reveals the origin of stronger localization of lateral distributions (Fig. 5). In comparison of $\theta = 3/8$ and $\theta = 4/8$ the statistical factor, $N_{\text{sim}}/N_{\text{fcc}}$ in Table 2 should be taken into account. At coverage $\theta = 3/8$, the temperature dependence is relatively small.

The pair correlation function in the non-periodic z-direction shows only Gaussian type behavior, similar to that of the case of single-adsorbate [18].

The classical hydrogen pair correlation distributions are similar to those of quantum adsorbates, the only

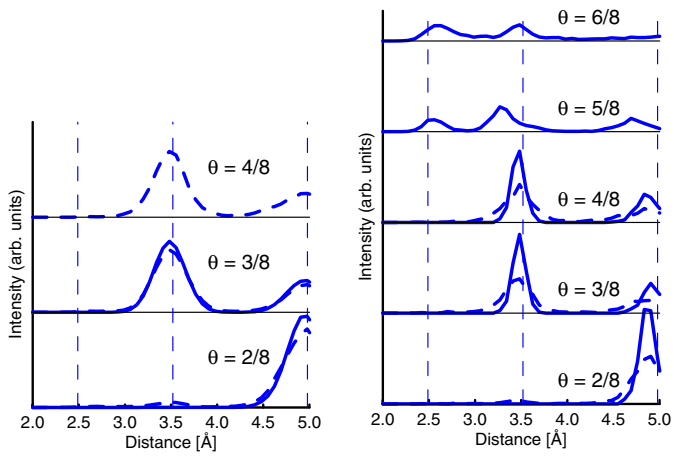

Fig. 7. Pair correlation function of H adsorbates corresponding to the one-particle distributions in Figs. 5 and 6, quantum case to the left and classical to the right. The two temperatures $T = 100$ K (solid line) and at $T = 300$ K (dashed line) are shown. Vertical dashed lines indicate the three hollow site distances, shown in Fig. 1.

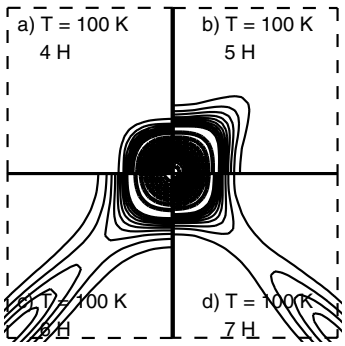

Fig. 8. "Classical hydrogen" distributions of higher coverages. Here, only temperature $T = 100$ K is shown, because at higher temperatures, the system becomes unstable. This is the case for coverage $\theta = 7/8$ even at $T = 100$ K.

essential difference being that quantum peaks are broader than classical peaks, see Fig. 7, revealing the quantum delocalization.

The hydrogen lateral distributions of higher coverages, $\theta = 4/8$–$7/8$, are shown in Fig. 8. We considered these with classical adsorbates only. For coverages $\theta > 4/8$, the hydrogen adsorbates are recombined and desorption of H_2 molecule occurs at $T = 300$ K. This may be an artifact of too small chemisorption energy of MBA, as higher coverages of quantum adsorbates are observed [1,16,17,36] and used in DFT calculations [12,25]. At $T = 100$ K, the coverages $\theta < 7/8$ are stable. The pair correlation functions of higher coverages (Fig. 7) show that adsorbates start to occupy the nearest hollow sites too.

Here, the location of maximum in z-distribution gets higher from 0.47 Å for 2 H atoms via 0.58 Å for 5 H adsorbates to 0.64 Å for 6 and 7 adsorbates. The z-distribution is not Gaussian for high coverages, as for the lower coverages, but reveals also another peak at a potential-energy minimum, $z = 1.1$ Å, which can be identified in the elbow plots in Fig. 3.

3.3. Energetics

Evaluation of energetics turns out to be a real computational challenge. This is due to extremely slow convergence to equilibrium with stationary energetics. Although, the distributions seem to converge faster by visual judgement, those above have been evaluated from the fully converged equilibrium. For the energetics below, with chosen Trotter number $M = 64$, we were able to acquire data, enough to make the statistical error bars negligible with respect to the convergence in Trotter number. In case of several H adsorbates, we are not able to evaluate the latter, but from the case of a single adsorbate [18], we estimate this "systematic error" to be of the order of a few meV.

As the MBA potential does not involve pair interactions, the interaction energy between two atoms, e.g., H–H interaction, cannot be evaluated directly. To estimate that, we used the total MBA potential of N hydrogen adsorbates energy

$$E_{\mathrm{pot},N}(\beta) = E_{\mathrm{T}} \tag{5a}$$

obtained directly from simulations, by Eq. (1), and the single-adsorbate potential energy $E_{\mathrm{pot},1}$ of the three-dimensional density function $\rho(r)$ of N hydrogen adsorbates as

$$E_{\mathrm{pot},1}(\beta) = \langle V_1(r)\rangle_{\rho(r)}, \tag{5b}$$

where $V_1(r)$ is taken to be single-adsorbate energy term, see Eq. (1). By comparing these two Eqs. (5a) and (5b), we are able to find an approximation to the interaction energy between H adsorbates.

We evaluated the kinetic energy via virial theorem, and only an approximation to that is used by assuming only single-hydrogen adsorbate, thus

$$E_{\mathrm{vir},1}(\beta) = \frac{1}{2}\langle r \cdot \nabla V_1(r)\rangle_{\rho(r)}.$$

This gives a good approximation as long as the H–H interaction is small, which is true for long-distance adsorbates on surface. From the pair correlation function, we conclude that the energetic estimates here are valid for at least H_2 and H_3. The total energy for single-adsorbate system is then

$$E_{\mathrm{tot},1} = E_{\mathrm{pot},1} + E_{\mathrm{vir},1}.$$

For the interacting system, by replacing the kinetic energy term with its single-adsorbate counterpart, we get the total energy

$$E_{\mathrm{tot},N} = E_{\mathrm{T}} + E_{\mathrm{vir}} \approx E_{\mathrm{T}} + E_{\mathrm{vir},1},$$

where E_{T} is given in Eq. (1), and thus, by writing the total energy in the form $E_{\mathrm{T}} = E_{\mathrm{pot},1} + E_{\mathrm{H-H}}$, we get an approximation for the interaction energy $E_{\mathrm{H-H}}$ of hydrogen adsorbates.

Next, we consider the energetics of hydrogen adsorbates on nickel surface.

Fig. 9a shows the variation of one-hydrogen potential energy $E_{\mathrm{pot},1}$ as a function of coverage θ. The potential energies for the quantum distributions are larger and the temperature effect is smaller compared to classical, as was pointed out earlier in discussion about the distributions. The maximum value is 90 meV at coverage 1/8. As was earlier pointed out, the H–H interaction pushes the lateral distributions smaller resulting in a smaller potential energy. The minimum potential energy of 75 meV is reached at coverage $\theta = 4/8$ for $T = 300$ K and 65 meV at $\theta = 3/8$ for $T = 100$ K.

The classical simulation shows considerable temperature effect. The single-particle potential energy of classical simulations with coverage 4/8 gives almost the same result than the quantum case. Here, it should be noticed that the lateral distributions of those two cases are very similar.

The single-adsorbate kinetic energy estimator is shown in Fig. 9b. The maximum value 100 meV is obtained at $\theta = 1/8$ and the energy is getting lower as the coverage is increasing. The minimum value is 60 meV for $T = 300$ K at $\theta = 4/8$. The quantum effect is rather large for kinetic energy also. At coverage of 4/8, the classical kinetic energy

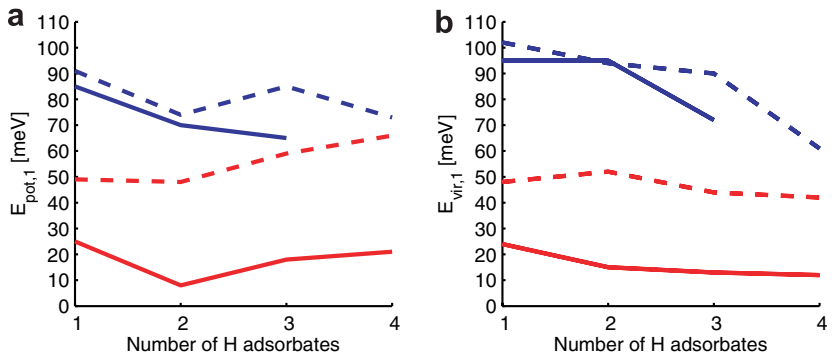

Fig. 9. Single-adsorbate approximation of potential energy (left) and kinetic energy (right) of hydrogen adsorbates on Ni surface. Solid line is for $T = 100$ K and dashed line for $T = 300$ K. Classical results are the lower (red), quantum statistical results are the upper (blue). The statistical error bars are hidden in the line width. (For interpretation of the references in colour in this figure legend, the reader is referred to the web version of this article.)

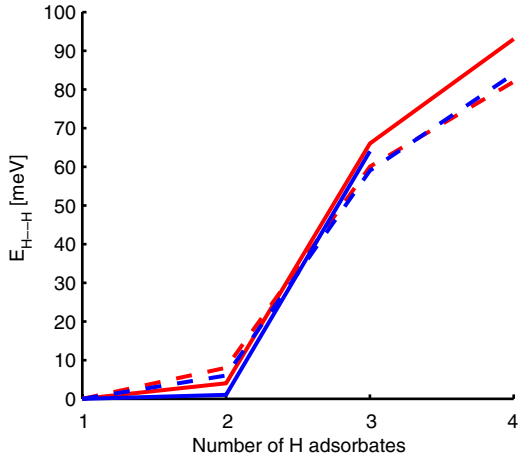

Fig. 10. Total interaction energy of the hydrogen adsorbates on Ni surface. Notations are the same as in Fig. 9.

is near to the quantum kinetic energy, when both are evaluated as a single-adsorbate approximation.

The interaction part of the potential term, Fig. 10 strongly depends on the number of adsorbates. The interaction energy increases from a few meV with two adsorbates to 100 meV with four hydrogen adsorbates in accordance with the above discussion of pair correlation function in Fig. 7 and energies given in Table 2. Only a small temperature dependence can be found. Quantum and classical interaction energies are rather similar.

4. Conclusions

We have carried out a study of quantum delocalization of hydrogen adsorbates on rigid Ni(0 0 1) surface at finite temperatures. Adsorbate distributions and energetics were determined at two temperatures, 100 K and 300 K, to trace the temperature dependencies.

To flexibly describe the adsorbate–substrate interaction and those between substrate and adsorbate atoms, we use the tight-binding derived MBA potential, which contains only a few parameters for atom pairs. The parameters were fitted to the adsorption energetics and geometries from DFT calculations. Path-integral Monte Carlo method is used, as it is a straightforward but computationally intensive approach to find the finite temperature mixed quantum state. The classical limit can be nicely found within the same formalism too.

We find strong quantum delocalization of the adsorbates at 100 K, the classical adsorbate being significantly more localized in terms of distribution and energetics. At this low temperature, the adsorbates are residing in the lateral "circular ground state", thus, showing harmonic confinement. For low coverages, $\theta \leqslant 3/8$, the distributions of classical adsorbates are more bridge-site oriented but for the coverage $\theta = 4/8$, the lateral distribution of classical and quantum cases are rather similar.

The hydrogen adsorbates have a repulsive interaction as they tend to reside apart from each other. No molecular H_2 state was found with the considered coverages. The quantum effect is mainly due to zero-point effects and tunneling towards Ni atoms in $\langle 1\,0\,0 \rangle$ directions.

The single-adsorbate potential and kinetic energies are not very sensitive to the hydrogen adsorbate coverage. Opposed to quantum case, the energetics of classical adsorbates have a considerable temperature effect, as is presumed from the distributions, already. The interaction energy of adsorbates has a strong dependence on hydrogen coverage. The interaction energy is independent of temperature and the type of the adsorbates, quantum or classical.

Acknowledgements

For financial support, the authors thank Graduate School of Tampere University of Technology and the Academy of Finland, and for computational resources, CSC, Center of Scientific Computing, Finland, and the M-grid facilities.

References

[1] K. Christmann, O. Schober, G. Ertl, M. Neumann, Adsorption of hydrogen on nickel single crystal surfaces, J. Chem. Phys. 60 (11) (1974) 4528.

[2] R. Baer, Y. Zeiri, R. Kosloff, Hydrogen transport in nickel(111), Phys. Rev. B 55 (16) (1997) 10952.
[3] B. Jackson, M. Persson, A quantum mechanical study of recombinative desorption of atomic hydrogen on a metal surface, J. Chem. Phys. 96 (3) (1992) 2378.
[4] G. Källén, G. Wahnström, Quantum treatment of H adsorbed on a Pt(111) surface, Phys. Rev. B 65 (3) (2002) 033406(4).
[5] Ş.C. Bădescu, P. Salo, T. Ala-Nissilä, S.C. Ying, K. Jacobi, Y. Wang, K. Bedürftig, G. Ertl, Energetics and vibrational states for hydrogen monolayer on Pt(111), Phys. Rev. Lett. 88 (13) (2002) 136101(4).
[6] B.M. Rice, B.C. Garrett, M.L. Koszykowski, S.M. Foiles, M.S. Daw, Kinetic isotope effects for hydrogen diffusion in bulk nickel and on nickel surfaces, J. Chem. Phys. 92 (1990) 775.
[7] S.E. Wonchoba, W.-P. Hu, D.G. Truhlar, Surface diffusion of H on Ni(100): Interpretation of the transition temperature, Phys. Rev. B 51 (15) (1995) 9985.
[8] L.Y. Chen, S.C. Ying, Theory of surface diffusion: Crossover from classical to quantum regime, Phys. Rev. Lett. 73 (5) (1994) 700.
[9] Ş.C. Bădescu, S.C. Ying, T. Ala-Nissilä, Quantum diffusion of H/Ni(111) through a Monte Carlo wave function formalism, Phys. Rev. Lett. 86 (22) (2001) 5092.
[10] T.R. Mattsson, U. Engberg, G. Wahnström, H diffusion on Ni(100): A quantum Monte Carlo simulation, Phys. Rev. Lett. 71 (16) (1993) 2615.
[11] T.R. Mattsson, G. Wahnström, Quantum Monte Carlo study of surface diffusion, Phys. Rev. B 31 (3) (1995) 1885.
[12] T. Mattsson, G. Wahnström, L. Bengtsson, B. Hammer, Quantum-mechanical calculation of H on Ni(001) using a model potential on first-principles calculations, Phys. Rev. B 56 (1997) 2258.
[13] M.J. Puska, R.M. Nieminen, M. Manninen, B. Chakraborty, S. Holloway, J.K. Nørskov, Quantum motion of chemisorbed hydrogen on Ni surfaces, Phys. Rev. Lett. 51 (1983) 1081.
[14] M.J. Puska, R.M. Nieminen, Hydrogen chemisorbed on nickel surfaces: A wave mechanical treatment of proton motion, Surf. Sci. 157 (1985) 413.
[15] S.W. Rick, D.L. Lynch, J.D. Doll, The quantum dynamics of hydrogen and deuterium on the Pd(111) surface: a path integral transition state theory study, J. Chem. Phys. 99 (10) (1993) 8183.
[16] X.D. Zhu, A. Lee, A. Wong, U. Linke, Surface diffusion of hydrogen on Ni(100): An experimental observation of quantum tunneling diffusion, Phys. Rev. Lett. 68 (12) (1992) 1862.
[17] A. Lee, X.D. Zhu, L. Deng, Observation of transition from over-barrier hopping to activated tunneling diffusion: H and D on Ni(100), Phys. Rev. B 46 (23) (1992) 15472.
[18] M. Leino, J. Nieminen, T. Rantala, Finite temperature quantum distribution of hydrogen adsorbate on nickel(001) surface, Surf. Sci. 600 (2006) 1860.
[19] Ş.C. Bădescu, K. Jacobi, Y. Wang, K. Bedürftig, G. Ertl, P. Salo, T. Ala-Nissilä, S.C. Ying, Vibrational states of a H monolayer on the Pt(111) surface, Phys. Rev. B 68 (2003) 205401(6).
[20] A. Winkler, Interaction of atomic hydrogen with metal surfaces, Appl. Phys. A 67 (1998) 637.
[21] A. Groß, C.M. Wei, M. Scheffler, Poisoning of hydrogen dissociation at Pd(100) by adsorbed sulfur studied by ab-initio quantum dynamics and ab-initio molecular dynamics, Surf. Sci. Lett. 416 (1998) L1095.
[22] G. Mills, H. Jónsson, Quantum and thermal effects in H_2 dissociative adsorption: evaluation of free energy barriers in multidimensional quantum systems, Phys. Rev. Lett. 72 (7) (1994) 1124.
[23] A. Wong, A. Lee, X.D. Zhu, Coverage dependence of quantum tunneling diffusion of hydrogen and deuterium on Ni(111), Phys. Rev. B 51 (7) (1995) 4418.
[24] C. Nyberg, C.G. Tengstål, Vibrational interaction between hydrogen atoms adsorbed on Pd(100), Phys. Rev. Lett. 50 (21) (1983) 1680.
[25] G. Kresse, J. Hafner, First-principles study of the adsorption of atomic H on Ni(111), (100) and (110), Surf. Sci. 459 (2000) 287.
[26] J.P. Muscat, Ordering of hydrogen overlayers on the (110) surfaces of nickel and palladium, Phys. Rev. B 34 (12) (1986) 8863.
[27] A.S. Mårtensson, C. Nyberg, S. Andersson, Observation of molecular H_2 chemisorption on a nickel surface, Phys. Rev. Lett. 57 (16) (1986) 2045.
[28] H. Grönbeck, D. Tománek, S.G. Kim, A. Rosén, Does hydrogen premelt palladium clusters? Chem. Phys. Lett. 264 (1997) 39.
[29] H. Grönbeck, D. Tománek, S.G. Kim, A. Rosén, Hydrogen induced melting of palladium clusters, Z. Phys. D 40 (1997) 469.
[30] W. Zhong, Y. Cai, D. Tománek, Mechanical stability of Pd–H systems: A molecular-dynamics study, Phys. Rev. B 46 (1992) 8099.
[31] W. Zhong, Y.S. Li, D. Tománek, Effect on adsorbates on surface phono modes: H on Pd(001) and Pd(110), Phys. Rev. B 44 (23) (1991) 13053.
[32] D.M. Ceperley, Path integrals in the theory of condensed helium, Rev. Mod. Phys. 67 (2) (1995) 279.
[33] M. Wagner, D.M. Ceperley, Path integral Monte Carlo simulations of thin ^{4}He films on a H_2 surface, J. Low Temp. Phys. 89 (3/4) (1992) 581.
[34] J. Rubio, M.C. Refolio, M.P.L. Sancho, J.M.L. Sancho, Correlation effects in photoemission from adsorbates: hydrogen on narrow-band metals, Phys. Rev. B 38 (5) (1988) 3142.
[35] G. Kresse, Dissociation and sticking of H_2 in the Ni(111), (100) and (110) substrate, Phys. Rev. B 62 (12) (2000) 8295.
[36] T. Kammler, S. Wehner, J. Küppers, Interaction of thermal H atoms with Ni(100)–H surfaces; through surface penetration and adsorbed hydrogen abstraction, Surf. Sci. 339 (1995) 125.